Journal of Engineering Mechanics and Machinery (2026)
Clausius Scientific Press, Canada

DOI: 10.23977/jemm.2026.110204
ISSN 2371-9133 Vol. 11 Num. 2

Multi-Condition Dynamic Transmission Error and Applicability Boundaries of a Simplified Model for Harmonic Reducers with Flexible Bearing Support

Runjie Li, Junhua Bao*

Dalian Jiaotong University, Dalian, Liaoning, China
**Corresponding Author*

Keywords: Harmonic reducer, flexible bearing, detrended dynamic transmission error, multibody dynamics, frequency-domain analysis

Abstract: To clarify the effect of flexible bearing support on the dynamic transmission error of harmonic reducers, this study established a multibody dynamic model incorporating the flexible bearing support path and used a cam-direct support model as the simplified comparator. The model was developed through APDL parametric modeling and RecurDyn dynamic simulation, and the input and output angular displacement responses were extracted under multiple input speeds and output loads. For the angular displacement data in the steady-state window, the detrended dynamic transmission error TE^{*} was further defined by linearly fitting the input and output angular displacements, and TE^{*}_{RMS}, $TE^{*}_{P\text{-}P}$, and the output-speed fluctuation coefficient were used to evaluate the dynamic transmission performance. The results show that the flexible bearing support model produces a stronger periodic dynamic error response under medium and high loads. In contrast, the cam-direct support model weakens the error amplification induced by the flexible support path. These findings provide a basis for wave-generator support modeling, simplified-model selection, and multi-condition dynamic performance evaluation of harmonic reducers.

1. Introduction

Harmonic reducers, also known as strain wave gear drives, are compact precision transmissions that achieve high reduction ratios, coaxial input-output motion and fine positioning capability through the controlled elastic deformation of a flexspline. These characteristics make them widely used in robot joints, precision servo actuators, aerospace mechanisms and other high-performance motion systems. Recent studies have examined their kinematic accuracy in space mechanisms[1] and have emphasized that transmission error is a direct indicator of positioning accuracy and control quality[2]. As operating speed, load level and control bandwidth increase, harmonic reducers are no longer evaluated only by static reduction ratio or nominal positioning accuracy. Their nonlinear dynamic response, torsional compliance and output-speed fluctuation increasingly determine whether a joint can maintain smooth and repeatable motion under service conditions[3].

Previous work has clarified several sources of error in harmonic drives. Dong et al. developed an

equivalent mechanism model to analyze kinematic accuracy, showing that geometric relationships and component deformation influence transmission accuracy[4]. Cheng and Chen further investigated tooth profile design and optimization, demonstrating that wave-generator geometry, tooth engagement and profile parameters can change the error behavior of strain wave gears[5]. These studies established important links between reducer geometry and accuracy, but most of them treat the wave-generator support condition as a simplified boundary or focus mainly on geometric and kinematic error. For dynamic transmission error under multiple operating conditions, the influence of the actual support path between the cam, flexible bearing and flexspline remains insufficiently separated from the influence of tooth geometry and flexspline deformation.

The flexible bearing is a particularly important part of this support path. Li et al. analyzed the load distribution of thin-walled flexible bearings in harmonic reducers while considering assembly with the flexspline and cam, indicating that the bearing is not merely a passive support component[6]. Hu et al. modeled the torsional stiffness of the flexspline-flexible bearing contact pair and showed that contact behavior across scales affects reducer stiffness[7]. Zhao et al. studied dynamic modeling and fault diagnosis of flexible thin-walled elliptical bearings, further highlighting the dynamic role of the bearing in harmonic reducers[8]. Wang et al. also analyzed thin-walled flexible components and showed that their deformation characteristics are closely related to reducer mechanical performance[9]. Together, these studies suggest that the flexible bearing may alter local displacement coordination, equivalent support stiffness and load-transfer behavior. However, they do not directly answer how much dynamic transmission error is changed when the flexible bearing support path is omitted from a multibody model.

Finite-element and multibody modeling provide a practical route for addressing this question. General mathematical and finite-element models of strain wave gears have been used to represent complex tooth profiles and elastic deformation[10]. At the system level, recent work on dynamic torsional stiffness, flexspline structural design, transmission-error prediction and vibration of thin-walled bearings has shown that speed, load, structural compliance[11] and periodic excitation can jointly affect reducer accuracy and vibration response[12]. These findings imply that a simplified cam-direct support model may be useful for rapid engineering simulation.

We therefore hypothesize that the flexible bearing support path is not a neutral modeling detail in the dynamic evaluation of harmonic reducers. Specifically, we expect that replacing the cam-flexible bearing-flexspline path with a cam-direct support model will reduce the apparent compliance and contact coordination in the wave-generator support system. As a result, the simplified model should underestimate the amplitude, peak-to-peak range, load sensitivity and dominant periodic component of the detrended dynamic transmission error, especially under medium and high output loads.

To test this hypothesis, this study establishes two multibody dynamic models of a cup-type harmonic reducer: a flexible bearing support model and a cam-direct support simplified model. The models are constructed through APDL parametric modeling and RecurDyn simulation, and the input and output angular displacement responses are extracted under multiple input speeds and output loads. To distinguish the average transmission relationship from dynamic fluctuation, the output angular displacement is fitted against the input angular displacement in a common steady-state window, and a detrended dynamic transmission error is defined. The root-mean-square value, peak-to-peak value, output-speed fluctuation coefficient and dominant frequency-domain peak are then used to compare the two support models. This work aims to define the applicability boundary of the simplified model and to provide modeling guidance for harmonic reducer simulation under flexible bearing support.

2. Harmonic reducer structure and two support models

2.1 Structural composition and main parameters

The object of this study is a cup-type harmonic reducer, which mainly consists of a circular spline, a flexspline, and a wave generator. The circular spline is an internal-tooth component, and the flexspline is a thin-walled cup-shaped elastic component with external teeth. The wave generator produces periodic radial deformation of the flexspline through elliptical support and forms local meshing between the flexspline and circular spline near the major axis. In the flexible bearing support model, the flexible bearing is an important component of the wave generator. Its outer ring deforms with the elliptical cam and transfers the deformation to the inner wall of the flexspline. In the cam-direct support simplified model, the flexible bearing is omitted, and the cam directly applies equivalent radial deformation to the flexspline. The main structural parameters used in this study are listed in Table 1.

Table 1. Main structural parameters of the harmonic reducer

Parameter	Symbol	Value
Module	m	0.24534 mm
Normal pressure angle	a_n	20 °
Addendum coefficient	h_a^*	0.725586941
Number of flexspline teeth	Z_f	200
Number of circular spline teeth	Z_c	202
Tooth width	b	8 mm
Flexspline wall thickness under	t_f	0.586 mm
Theoretical speed ratio	i	-0.01

2.2 Transmission principle and transmission ratio

When the circular spline is fixed, the wave generator is used as the input, and the flexspline is used as the output, the output rotational speed of the flexspline is opposite in direction to the input rotational speed of the wave generator. If the ratio of the input angular displacement increment to the output angular displacement increment is defined as the nominal transmission ratio, then:

$$i = \frac{\omega_{in}}{\omega_{out}} = \frac{Z_f}{Z_f - Z_c} \tag{1}$$

Substituting Z_f=200 and Z_c=202 gives $i = -100$. The negative sign indicates that the output end rotates in the opposite direction to the input end.

From an idealized geometric perspective, the action of the wave generator on the flexspline can be approximated as a second-harmonic radial displacement distributed along the circumference:

$$u_r(\varphi)=w_0\cos(2\varphi) \tag{2}$$

In this expression, $u_r(\varphi)$ is the radial displacement of the flexspline at circumferential angular position φ, and w_0 is the maximum radial displacement of the wave generator or drive end

2.3 Two support models and theoretical differences

To analyze the effect of the wave-generator support mode on dynamic transmission performance,

a flexible bearing support model (B) and a cam-direct support simplified model (NB) were established. The main differences between the two models are shown in Table 2.

Table 2. Comparison of the two support models and their characteristics

Model abbreviation	Model name	Support mode	Load-transfer path
B	Flexible bearing support model	The cam supports the flexspline through the flexible bearing	Cam to flexible bearing to flexspline to circular spline
NB	Cam-direct support simplified model	The rigid cam directly supports the flexspline	Cam to flexspline to circular spline

The two models differ in their support path, equivalent stiffness, and local deformation coordination. If the local equivalent stiffness of the flexspline is denoted as k_f, the equivalent stiffness of the cam support as k_c, and the equivalent stiffness of the flexible bearing as k_b, the cam-direct support model can be approximately regarded as a series relationship between cam support and local flexspline deformation:

$$\frac{1}{k_{NB}}=\frac{1}{k_c}+\frac{1}{k_f} \tag{3}$$

In the flexible bearing support model, the flexible bearing is located between the cam and the flexspline, and its equivalent stiffness can be approximately expressed as:

$$\frac{1}{k_B}=\frac{1}{k_c}+\frac{1}{k_b}+\frac{1}{k_f} \tag{4}$$

When the cam stiffness is much greater than the local stiffnesses of the flexible bearing and flexspline, the flexible bearing support model usually has lower equivalent stiffness and is therefore more prone to additional deformation and amplified dynamic response under load.

3. Dynamic modeling and error evaluation method

APDL was used to parametrically model the flexspline, circular spline, cam support body, and flexible-bearing-related structures, and the model was imported into RecurDyn for multibody dynamic simulation. The unit system of the model was N-kg-mm-s. Key components were introduced into the dynamic solution as FFlex/NFlex flexible bodies to reflect the influence of thin-walled components and support-path flexibility on the system dynamic response.

To compare the influence of the flexible bearing support path on the dynamic response, two RecurDyn multibody dynamic models were established, as shown in Figure 1. In the cam-direct support simplified model, the cam directly applies equivalent radial support to the inner wall of the flexspline. In the flexible bearing support model, the elliptical deformation of the cam is transmitted to the flexspline through the flexible bearing. Both models include the circular spline, flexspline, and wave-generator-related structures, and the input and output angular displacement responses were extracted under the same operating conditions for subsequent dynamic transmission error analysis.

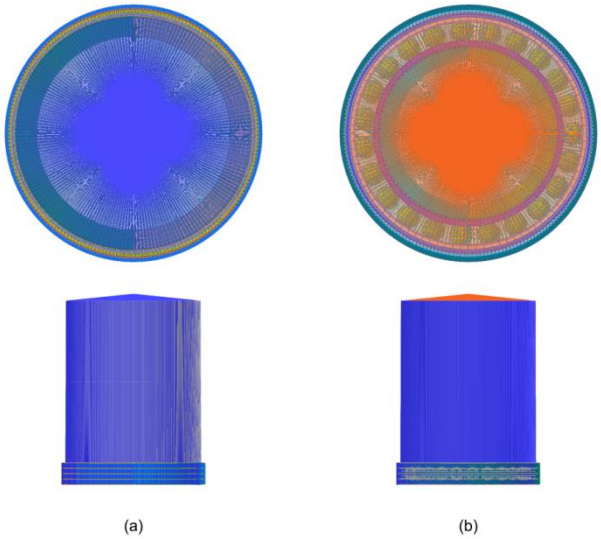

Figure 1. RecurDyn multibody dynamic models of the harmonic reducer: (a) cam-direct support simplified model; (b) flexible bearing support model.

3.1 Model settings and solution

The main material parameters of the two models are listed in Table 3. In the bearing-supported model, the flexible bearing has independent material parameters. Therefore, the NB model is positioned in this study as a simplified reference model. The Main material parameters of the two models are shown in Table 3.Contact parameter settings used in the dynamic simulation are shown in Table 4.

Table 3. Main material parameters of the two models

Model	Component	Elastic modulus E/(Mpa)	Shear modulus G/(Mpa)	Poisson's ratio ν
NB	zg	174000	68503.94	0.270
	zr	204000	79069.77	0.290
	tulun1/2	211000	82615.51	0.277
B	zg	174000	68503.94	0.270
	zr	204000	79069.77	0.290
	tulun1/2	211000	82615.51	0.277
	bear	219000	84883.72	0.290

Table 4. Contact parameter settings used in the dynamic simulation

Contact pair	Applied model	Normal stiffness parameter K	Damping parameter C	Friction coefficient μ
Circular spline–flexspline	B/NB	100	0.01	0.08
Cam–flexspline	NB	100	0.01	0.15
Cam–bearing	B	100	0.01	0.15
Bearing–flexspline	B	100	0.01	0.15
Ball–retainer contact	B	10	0.0001	0

Contact parameters are important factors affecting the dynamic response. Both models include circular-spline-flexspline contact, the NB model includes cam-flexspline contact, and the B model further includes cam-bearing and bearing-flexspline contact.

In the simulation, the circular spline was fixed, an input-speed drive was applied at the wave-

generator end, and load torque was applied at the output end. The input speed and output torque were both smoothly loaded using a STEP function to reduce the influence of the initial impact on the steady-state response. Different speed and load conditions were generated by parametrically modifying the target speed n and target torque T. The input-speed function can be written as:

$$\omega_{in}(t)=\mathrm{STEP}(t,0,0,2l_d,\frac{2\pi n}{60}) \tag{5}$$

Here, $l_d = 0.02$ s, so the speed drive reaches the target value within 0-0.04 s. The output torque is also loaded to the target load within 0.02-0.04 s. Because the displacement in the B model must be transmitted to the flexspline through the flexible bearing and contact interfaces, this drive-end displacement is not equivalent to the actual radial deformation of the flexspline. In the NB model, it is the equivalent radial displacement input when the cam directly supports the flexspline.

3.2 Operating conditions

Two types of simulation conditions were set in this study: speed conditions and load conditions. For the speed conditions, the output load was fixed at 50 $\mathrm{N \cdot m}$, and the input speeds were 1000, 1500, 2000, and 2500 $\mathrm{r \cdot min^{-1}}$. For the load conditions, the input speed was fixed at 2000 $\mathrm{r \cdot min^{-1}}$, and the output loads were 0, 12.5, 25, 37.5, and 50 $\mathrm{N \cdot m}$. The loading function was completed before 0.04 s. To reduce the influence of the start-up transient on the evaluation indices, the steady-state window was selected as $t = 0.05 - 0.1s$ after the completion of the loading process. The same time window was used for all statistical and frequency-domain analyses. The specific operating conditions are shown in Table 5.

Table 5. Operating-condition settings

Condition type	Model	Input speed/($\mathrm{r \cdot min^{-1}}$)	Output load/($\mathrm{N \cdot m}$)
Speed condition	B/NB	1000, 1500, 2000, 2500	50
Load condition	B/NB	2000	0, 12.5, 25, 37.5, 50

3.3 Angular velocity, steady-state window, and transmission-ratio fitting

Let the input-end angular displacement be $\theta_{in}(t)$, and the output-end angular displacement be $\theta_{out}(t)$. To distinguish the average transmission relationship from dynamic fluctuation, the input and output angular displacements in the steady-state window were linearly fitted:

$$\theta_{out}(t)\approx a\theta_{in}(t)+b \tag{6}$$

In the equation, a represents the average speed ratio in the steady-state window, and b absorbs the initial phase and zero-position offset. The detrended dynamic transmission error is therefore defined as:

$$TE^{*}(t)=3600\left[\theta_{out}(t)-a\theta_{in}(t)-b\right] \tag{7}$$

It should be noted that TE^{*} represents the fluctuation component after removing the fitted average transmission trend. Therefore, it is mainly used to evaluate steady-state dynamic fluctuation rather than the absolute kinematic transmission error.

The root-mean-square value and peak-to-peak value of the dynamic transmission error are respectively defined as:

$$TE^{*}_{RMS}=\sqrt{\frac{1}{N}\sum_{n=0}^{N-1}[TE^{*}(n)]^{2}} \tag{8}$$

$$TE^{*}_{P-P}=TE^{*}_{max}-TE^{*}_{min} \tag{9}$$

To evaluate output smoothness, the output angular-velocity fluctuation coefficient is defined as:

$$C_v=\frac{\sigma_\omega}{|\overline{\omega}_{out}|} \tag{10}$$

Here, σ_ω is the standard deviation of the output angular velocity, and $\overline{\omega}_{out}$ is the mean output angular velocity.

3.4 Frequency-domain amplitude spectrum and dominant peak extraction

The discrete Fourier transform converts discrete sampling points in the time domain into discrete points in the frequency domain. Although the number of sample points is finite, the sampled signals in both the time domain and the frequency domain are usually regarded as principal value sequences of discrete periodic signals. Through periodic extension, a finite-length time-domain signal can be converted into a periodic signal. In practical applications, the fast Fourier transform has been widely used.

To further reveal the frequency composition and dominant response characteristics of dynamic error in the two models under different operating conditions, the dynamic transmission error signal $TE^{*}(n)$ was analyzed in the frequency domain. The complex spectrum obtained by the discrete Fourier transform is:

$$X(k)=\sum_{n=0}^{N-1} T\,E^{*}(n)W_N^{kn} \tag{11}$$

In the expression, $W_N=e^{-j\frac{2\pi}{N}}$, and N is the length of the transform interval.

4. Simulation results and discussion

4.1 Dynamic transmission performance under different speed conditions

With the output load fixed at 50 N · m, dynamic simulations were conducted for the B and NB models at input speeds of 1000, 1500, 2000, and 2500 $r\cdot min^{-1}$. The corresponding results obtained from the fitted input and output angular displacements in the common steady-state window are shown in Table 6.

Table 6. Dynamic transmission performance under different speed conditions

Model type	$n/r\cdot min^{-1}$	T/N·m	TE^{*}_{RMS}/(arcsec)	TE^{*}_{P-P}/(arcsec)	C_v
B model	1000	50	12.938	52.713	0.054371
	1500	50	14.835	58.685	0.047066
	2000	50	15.597	53.977	0.041319
	2500	50	13.716	54.351	0.030656
NB model	1000	50	2.801	11.342	0.020463
	1500	50	2.417	13.577	0.015429
	2000	50	6.674	25.028	0.036543
	2500	50	1.794	8.878	0.006990

As shown in Table 6, under a load of 50 N · m, the flexible bearing support model exhibits higher dynamic transmission error amplitudes at all speed conditions. Its TE^{*}_{RMS} remains within 12.938-15.597 arcsec, whereas that of the cam-direct support simplified model is only 1.794-6.674 arcsec. The TE^{*}_{P-P}also increases from 8.878-25.028 arcsec in the simplified model to 52.713-58.685 arcsec in the flexible bearing support model. At the same speed, the TE^{*}_{RMS} of the flexible bearing support model is approximately 2.34-7.65 times that of the simplified model, and the TE^{*}_{P-P} is approximately 2.16-6.12 times that of the simplified model. This result indicates that, under the same load, the flexible bearing support path significantly enhances the dynamic fluctuation of output angular displacement relative to the fitted average transmission relationship.

The output-speed fluctuation coefficient also shows a clear difference between the support models. The output-speed CV of the flexible bearing support model is 0.030656-0.054371, which is generally higher than the 0.006990-0.036543 of the simplified model. With increasing input speed, the error amplitude of the B model first increases and then decreases slightly, reaching a relatively high level near 2000 r · min^{-1}. The NB model also shows a local increase near 2000 r · min^{-1}, but its overall amplitude is much lower than that of the B model. This indicates that speed variation changes the dynamic response level of the system, but its effect is not simply monotonic and may be related to the coupling among contact state, support flexibility, and periodic excitation frequency.

4.2 Dynamic transmission performance under different load conditions

With the input speed fixed at 2000 r · min^{-1}, dynamic simulations were conducted for the two models under output loads of 0, 12.5, 25, 37.5, and 50 N · m. The statistical indices under different load conditions are shown in

Table 7. Dynamic transmission performance under different load conditions

Model type	Inputspeed/$r{\cdot}min^{-1}$	T/N · m	TE^{*}_{RMS}/(arcsec)	TE^{*}_{P-P}/(arcsec)	C_v
B model	2000	0.0	4.604	19.045	0.015157
	2000	12.5	8.717	33.466	0.025897
	2000	25.0	9.055	40.470	0.025088
	2000	37.5	11.160	42.445	0.031054
	2000	50.0	15.597	53.977	0.041319
NB model	2000	0.0	9.218	37.746	0.043986
	2000	12.5	6.468	26.626	0.033762
	2000	25.0	4.895	19.372	0.025947
	2000	37.5	5.481	20.102	0.029350
	2000	50.0	6.674	25.028	0.036543

As shown in Table 7, at an input speed of 2000 r · min^{-1}, load variation has a more significant effect on the dynamic transmission performance of the flexible bearing support model. As the load increases from 0 N · m to 50 N · m, the $TE^{*}_{RMS}$of the B model increases from 4.604 arcsec to 15.597 arcsec, corresponding to an increase of approximately 238.8%. The TE^{*}_{P-P} increases from 19.045 arcsec to 53.977 arcsec, corresponding to an increase of approximately 183.4%. The output-speed fluctuation coefficient increases from 0.015157 to 0.041319, corresponding to an increase of approximately 172.6%. This result indicates that increasing load not only changes the average transmission state, but also continuously amplifies the amplitude, extreme-value range, and output-speed fluctuation of the detrended dynamic transmission error.

By contrast, the NB model has a relatively high TE^{*}_{RMS} of 9.218 arcsec under the no-load condition. After loading, it remains mostly within 4.895-6.674 arcsec, which is clearly lower than

that of the B model under the same loads. Its $TE^{*}_{P\text{-}P}$ is mainly within 19.372-26.626 arcsec after loading, which is also lower than the corresponding results of the flexible bearing support model. This phenomenon indicates that the cam-direct support simplified model cannot stably reflect the load sensitivity of the flexible bearing support path and will underestimate dynamic error amplification, especially under medium and high loads. The relatively high error of the NB model under the no-load condition suggests that direct support contact and boundary constraints may introduce local excitation different from that in the actual flexible bearing path, which should be further verified in subsequent experiments or parameter-sensitivity analyses.

Mechanistically, increasing load changes the local meshing force state between the flexspline and circular spline and affects local displacement transfer and contact coordination through the cam-flexible bearing-flexspline path. At higher loads, the additional compliance of the flexible bearing is superimposed on local flexspline deformation, causing dynamic error to be amplified during transmission. Therefore, the flexible bearing is not merely a support boundary, but a load-transfer element that participates in the generation and amplification of dynamic error.

4.3 Time and frequency-domain responses of the flexible bearing support model

To further reveal the effect of load variation on the frequency composition of dynamic error, the TE^{*} signals of the B model at 2000 $r \cdot min^{-1}$ under different loads were jointly analyzed in the time and frequency domains, as shown in Figure 2.

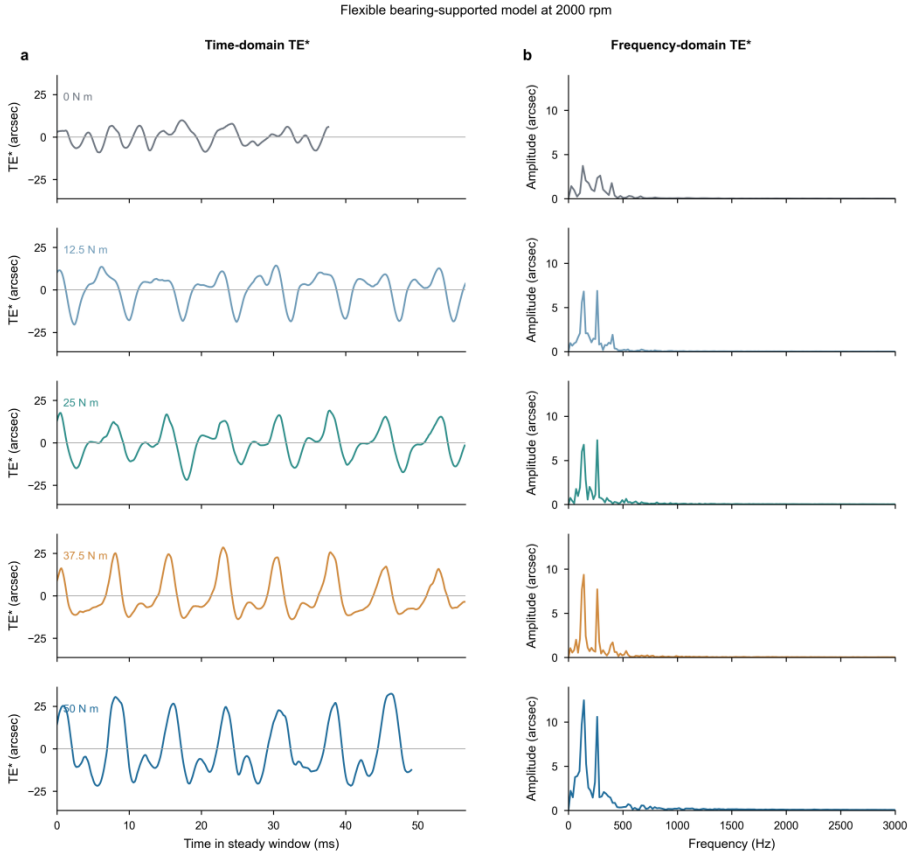

Figure 2. Time-domain TE^{*} curves and frequency-domain amplitude spectra of the flexible bearing support model at 2000 $r \cdot min^{-1}$.

As shown in Figure 2, the time-domain responses of the flexible bearing support model under different loads show clear load dependence. Under no load, the fluctuation amplitude is relatively

small. As the load increases, the periodic fluctuation of the time-domain waveform gradually intensifies and reaches its maximum at 50 N · m. This trend is consistent with the statistical indices in Figure 2, indicating that high load mainly appears as an enlargement of the dynamic error fluctuation amplitude rather than a single offset in the average transmission relationship.

The frequency-domain results further show that the main energy of the flexible bearing support model is concentrated in the low-frequency range. The dominant spectral peak amplitude increases from 3.71 arcsec under no load to 12.47 arcsec at 50 N · m, corresponding to an increase of approximately 236.1%. This result indicates that increasing load not only enlarges the time-domain error amplitude, but also simultaneously strengthens the response intensity at the main frequency component. Therefore, flexible bearing support under medium and high loads produces a stronger periodic dynamic transmission error response.

4.4 Time and frequency-domain responses of the cam-direct support simplified model

To compare the response characteristics of the simplified model under load conditions, Figure 3 presents the time-domain curves and frequency-domain amplitude spectra of the TE^* signal for the NB model at 2000 $r \cdot min^{-1}$ under different loads.

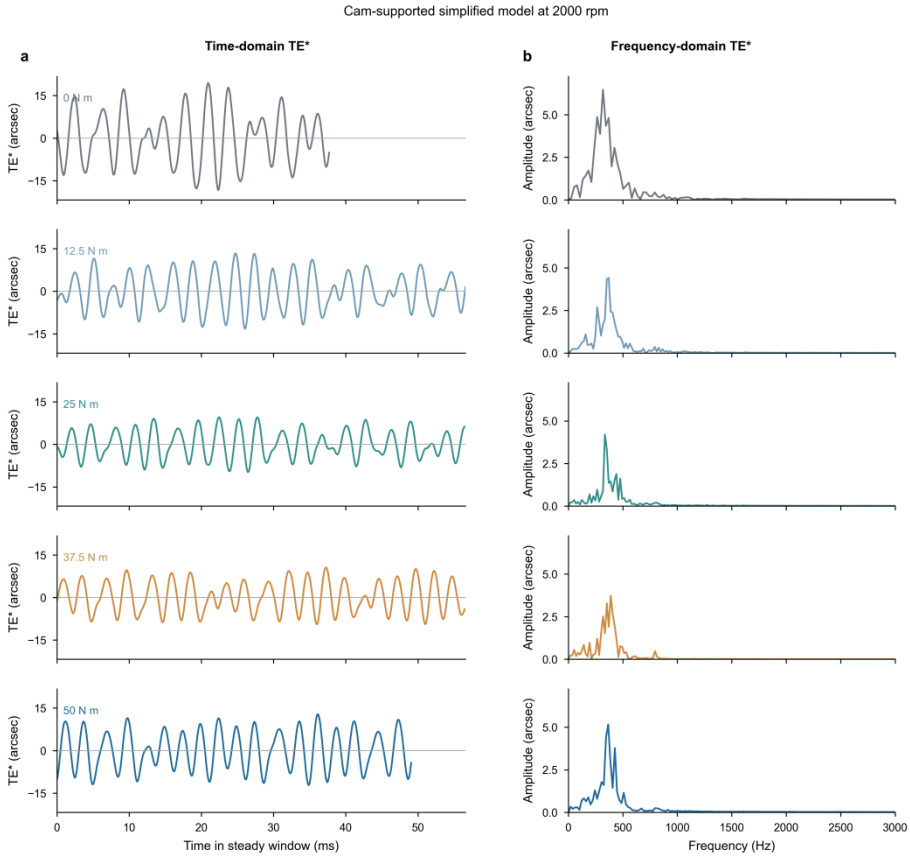

Figure 3. Time-domain TE^* curves and frequency-domain amplitude spectra of the cam-direct support simplified model at 2000 $\mathbf{r \cdot min^{-1}}$.

As shown in Figure 3, the response of the cam-direct support simplified model under different loads is generally weaker than that of the flexible bearing support model. Except under the no-load condition, the TE^*_{RMS} and $TE^*_{P\text{-}P}$ of this model under loaded conditions are lower than those of the flexible bearing support model under the same loads. This indicates that after the flexible bearing is omitted, the support flexibility, contact-transfer path, and local deformation coordination in the

model are weakened, resulting in a smaller dynamic error amplitude.

The frequency-domain results show that the dominant spectral peaks of the simplified model are mainly concentrated within 317-389 Hz, with amplitudes of 3.72-6.47 arcsec, which are generally lower than the spectral peak amplitudes of the flexible bearing support model under high loads. Thus, the cam-direct support simplified model can reflect the basic fluctuation pattern of dynamic transmission error, but it weakens the error amplification characteristics under flexible support conditions. The relatively high fluctuation of this model under the no-load condition should be discussed as a special case and should not be used to infer that it has a higher error level under loaded conditions.

4.5 Applicability boundaries of the simplified model

A synthesis of the time-domain statistical indices and frequency-domain dominant-peak results shows that the cam-direct support simplified model can be used for early-stage scheme comparison, low-cost trend judgment, or rapid simulation when the average transmission relationship is not sensitive. However, in medium- and high-load cases, speed-fluctuation evaluation, extreme-value prediction of dynamic transmission error, and assessment of the flexible support path, this model markedly weakens the error amplification characteristics. Therefore, when the research objective involves output smoothness, positioning accuracy, or high-load service performance, a model incorporating the flexible bearing support path should be preferred. If the simplified model is used, its applicability should be checked through error margins, parameter-sensitivity analysis, or experimental results.

5. Conclusions

Based on APDL parametric modeling and RecurDyn multibody dynamic simulation, this study investigated the dynamic transmission error characteristics of a harmonic reducer with flexible bearing support under multiple speeds and loads, and compared them with those of a cam-direct support simplified model. The main conclusions are as follows:

(1) Under a load of 50 N · m, the $TE^{*}_{RMS}$of the flexible bearing support model is 12.938-15.597 arcsec, approximately 2.34-7.65 times that of the cam-direct support simplified model. The $TE^{*}_{P\text{-}P}$ is 52.713-58.685 arcsec, approximately 2.16-6.12 times that of the simplified model. The flexible bearing support path significantly enhances dynamic transmission error fluctuation.

(2) Load has a more continuous and significant effect on the flexible bearing support model. When the load increases from 0 N · m to 50 N · m, the TE^{*}_{RMS}, $TE^{*}_{P\text{-}P}$, and output-speed fluctuation coefficient increase by approximately 238.8%, 183.4%, and 172.6%, respectively. This indicates that increasing load synchronously amplifies the error amplitude, extreme-value range, and output-speed fluctuation.

(3) The frequency-domain analysis shows that the dominant spectral peak amplitude of the flexible bearing support model increases markedly under high load, rising from 3.71 arcsec under no load to 12.47 arcsec at 50 N · m. The dominant peak amplitude of the simplified model is only 3.72-6.47 arcsec. The flexible support path amplifies periodic dynamic transmission error.

(4) The cam-direct support simplified model can reflect the basic fluctuation form of dynamic transmission error, but it underestimates the amplitude and load sensitivity under flexible bearing support conditions. This model is more suitable for early-stage scheme screening or low-load trend analysis and should not be used directly for medium- and high-load accuracy prediction or output-smoothness evaluation.

Compared with previous studies that mainly focused on flexspline deformation, kinematic error,

torsional stiffness, bearing load distribution, or error measurement separately, this work links the support path, load sensitivity, time-domain error indices, and frequency-domain response within a unified multibody dynamic evaluation.

Several limitations remain. The present work is based mainly on numerical simulation, and the effects of bearing-flexspline contact parameters, friction, manufacturing errors, assembly deviations, and thermal deformation have not been fully coupled with experimental validation. Future work should combine prototype testing, parameter-sensitivity analysis, and model correction to quantify the error margins of the simplified model and to develop calibrated correction factors for engineering design. Such work would further improve the reliability of dynamic transmission error prediction for harmonic reducers operating under high-load and high-precision conditions.

References

[1] Jacek P ,Dominika S ,Andrzej P .Numerical Analysis of the Kinematic Accuracy of the Hermetic Harmonic Drive in Space Vehicles[J].Applied Sciences,2023,13(3):1694.DOI:10.3390/APP13031694.

[2] Zhang S ,Gao J ,Wang L , et al. A novel on-line approach for evaluating transmission errors in harmonic drives[J]. Advances in Mechanical Engineering,2024,16(9):DOI:10.1177/16878132241276666.

[3] Guida R ,Bertolino C A ,Martin D A , et al. A new computationally efficient model of the non-linear dynamics in harmonic drive reducers[J].Mechanism and Machine Theory,2025,209105992. DOI:10.1016/J.MECHMACHTHEORY.2025.105992.

[4] Huimin D ,Bo D ,Chu Z , et al. An equivalent mechanism model for kinematic accuracy analysis of harmonic drive[J]. Mechanism and Machine Theory,2022,173DOI:10.1016/J.MECHMACHTHEORY.2022.104825.

[5] Cheng, Yun-Hao, and Yi-Cheng Chen. "Design, analysis, and optimization of a strain wave gear with a novel tooth profile." Mechanism and Machine Theory 175 (2022): 104953.

[6] Xinzi L ,Chaosheng S ,Caichao Z , et al. Load analysis of thin-walled flexible bearing in harmonic reducer considering assembly with flexspline and cam[J].Mechanism and Machine Theory, 2023,180 DOI:10.1016/J.MECHMACHTHEORY.2022.105154.

[7] Qiushi H ,Heng L ,Guang W , et al. Research on torsional stiffness of flexspline-flexible bearing contact pair in harmonic drive based on macro-micro scale modeling[J].Frontiers in Materials, 2023,10 DOI:10.3389/FMATS.2023.1211019.

[8] Zhao Z ,Sun S ,Xu W , et al. Dynamics modeling and fault diagnosis of flexible thin-walled elliptical bearings in harmonic reducers[J].Measurement,2024,238115378.DOI:10.1016/J.MEASUREMENT.2024.115378.

[9] Yazhen W ,Yang Y ,Wuqiang J , et al. Static analysis of thin-walled flexible components in a harmonic reducer[J].Journal of Mechanical Science and Technology,2023,37(7):3631-3642.DOI:10.1007/S12206-023-0628-X.

[10] Hao Y C ,Cheng Y C .A general mathematical modeling and finite element analysis of a strain wave gear possessing a double-circular-arc-with-a-common-tangent profile[J]. Proceedings of the Institution of Mechanical Engineers, Part C: Journal of Mechanical Engineering Science,2023,237(1):223-236. DOI:10.1177/09544062221114574.

[11] Cheng H ,Shi Z ,Yu Z , et al. Dynamic Torsional Stiffness of Reducers and Its Testing Method[J].Applied Sciences, 2023,13(16):DOI:10.3390/APP13169277.

[12] Ruixing L ,Guangwu Z ,Delun L .Structural design of flexible wheel of harmonic reducer based on efficiency improvement[J].Mechanical Systems and Signal Processing,2023,201DOI:10.1016/J.YMSSP.2023.110677.